

Diffusion and melting in two dimensions: A quasielastic neutron scattering study of alkali metals in graphite

H. Zabel*

*Department of Physics and Materials Research Laboratory, University of Illinois at Urbana-Champaign,
1110 West Green Street, Urbana, Illinois 61801*

A. Magerl

Institut-Laue-Langevin, Grenoble CEDEX, France

J. J. Rush

National Institute for Standards and Technology, Gaithersburg, Maryland 20899

M. E. Misenheimer[†]

*Department of Physics and Materials Research Laboratory, University of Illinois at Urbana-Champaign,
1110 West Green Street, Urbana, Illinois 61801*

(Received 5 April 1989)

Using quasielastic neutron scattering, we have studied the self-diffusion of alkali-metal atoms in stage-1 and stage-2 graphite intercalation compounds. For stage-1 compounds the diffusion proceeds via jumps to potential wells provided by the graphite substrate potential. The activation energies for diffusion in LiC_6 and KC_8 are 1.0 and 0.18 eV, respectively, and agree very well with theoretical values derived by DiVincenzo and Mele [Phys. Rev. B **32**, 2538 (1985)] for the saddle-point energy between C—C bonds. The diffusion of alkali-metal atoms in stage-2 compounds is qualitatively very different from that in stage-1 compounds. The characteristics of the diffusive motion appear to be intermediate between those of a free liquid and a lattice liquid. The activation energies are considerably lower and compare with those of hydrogen in metals: $E_a = 0.126$, 0.063, and 0.077 eV for K, Rb, and Cs, respectively, in stage-2 compounds. Moreover, the stage-2 compounds exhibit a continuous melting transition, which extends over several hundred degrees centigrade. Over this temperature range, liquidlike diffusive motion and solidlike phonon excitations coexist. We argue that this behavior is characteristic of the melting of a two-dimensional structure on a periodic substrate.

I. INTRODUCTION

Graphite intercalation compounds (GIC's) promise to reveal an abundance of information on two-dimensional (2D) liquid dynamics in the presence of a periodic substrate potential. GIC's are layered materials in which the graphite and intercalate layers alternate in an ordered fashion along the normal to the plane (c axis).¹ The compounds are characterized by their stage index n , which is the number of graphite basal planes between any two consecutive intercalate planes. Changing the stage of the compound also changes the interaction of the intercalate species with the host substrate, which, in turn, will affect the 2D diffusion process in a fundamental way. While stage-1 compounds with strong substrate potentials are expected to exhibit lattice-liquid-type jump diffusivities, in higher-stage compounds a more continuous type of diffusive motion may prevail. Quasielastic neutron scattering (QENS) is a powerful tool for the study of atomic or molecular diffusion in solids and liquids.²⁻⁴ The wave-vector and temperature dependence of the central width of quasielastic spectra contains detailed information on the microscopic diffusion mechanism. We

have applied this method to the investigation of the liquid dynamics and melting processes in GIC's.

Graphite intercalation compounds represent a particularly favorable system for the investigation of 2D liquid dynamics via neutron scattering. First, the large number of intercalate layers residing in the bulk material render neutron inelastic-scattering studies from monolayers possible without applying surface-sensitive scattering techniques. Second, the host graphite layers are atomically flat, and therefore the interpretation of the results does not interfere with lattice defects, surface steps, and the like. Third, intercalate layers are atomically clean because the intercalation process is highly selective, which eliminates the need for ultra-high-vacuum systems.

In the following we restrict our discussion to alkali-metal GIC's of the stage-1 compounds LiC_6 , KC_8 , and RbC_8 , and the stage-2 compounds KC_{24} , RbC_{24} , and CsC_{24} . The structures and phase transitions of these compounds are rather well described and are reviewed in several places,^{5,6} most recently by Moss and Moret.⁷ In brief, the intercalates in stage-1 compounds form commensurate superstructures that melt at high temperatures into lattice liquids. Stage-2 compounds, in contrast, ex-

hibit discommensuration domain structures at low temperatures which can be described by triple particle-density waves induced by the competing alkali-metal-alkali-metal and alkali-metal-graphite interactions. Above the melting transitions, 2D liquidlike structure factors are observed which continue to reflect the modulation of the liquid density by the corrugated substrate potential.

Among the GIC's, those with alkali-metal atoms are most suitable for QENS studies of the 2D liquid dynamics because the intercalate layers are monatomic and comparatively simple. This is in contrast to molecular intercalates, which exhibit rotational and librational motions in addition to the translational diffusion of the particles, compounding the complexity of the data analysis. Nevertheless, several studies on the dynamics of molecules in GIC's have been reported recently⁸⁻¹⁰ and are reviewed by Magerl in Ref. 11.

The focus of the present work is on the diffusional motion of the intercalated alkali-metal atoms in thermal equilibrium. This must be distinguished from studies of diffusional processes which occur during intercalation or deintercalation of the compound,¹² during staging transformation,¹³⁻¹⁵ and during domain formation after rapid quenching.¹⁶ Here we will only consider the equilibrium situation with a constant number density of intercalate atoms per intercalate layer.

From the foregoing discussion it is evident that alkali-metal layers in graphite represent rather ideal realizations for the investigation of 2D structures and dynamics in the presence of competing interactions. In a seminal paper, Frank and van der Merwe¹⁷ provided the theoretical frame for describing competing interactions in 1D monolayers on periodic substrates. Depending on the ratio of the adsorbate-adsorbate and adsorbate-substrate interaction, the overlayer may assume a commensurate or an incommensurate solitonlike structures. More recently, Bunde and Dietrich¹⁸ have analyzed the commensurability effect of 1D liquids in a periodic medium using the Percus-Yevick approach for describing the static liquid properties. Plischke¹⁹ has extended this treatment to two dimensions and he applied the liquid model to alkali-metal GIC's by treating the long-range metal-metal interaction via a screened Coulomb potential. Although he does not take the graphite periodic substrate into account, Plischke obtains a reasonable agreement with orientationally averaged x-ray structure-factor measurements of the 2D intercalate liquids, but this calculation clearly lacks the structural details which become more evident upon comparison with single-crystal measurements of the highly anisotropic liquid structure factor (LSF).^{20,21} Subsequently, Reiter and Moss²² developed a 2D liquid theory using the same metal pair potential as Plischke, but explicitly including the periodic potential of the host. The effect of this potential on the 2D LSF is to induce static density modulations of the liquid pair correlation which show up as liquidlike halos around the *HKO* reflections of the host substrate as well as extra intensity contributions to the *HKO* Bragg reflections. Monte Carlo (MC) simulations of the LSF modulated by the sixfold substrate potential of the graphite plane were provided by

Plischke and Leckie,²³ DiVincenzo,²⁴ and recently by Chen, Karim, and Pettitt.²⁵ In all these works it is clearly seen that the simple isotropic LSF with central diffuse rings about the origin of the reciprocal lattice is modified in the presence of a sixfold potential and replicas of the LSF surface at all reciprocal-lattice vectors of the substrate. Chen *et al.*²⁵ also showed that with increasing temperature the intensity of the noncentral rings diminishes strongly and the overall structure factor becomes more isotropic.

Recently, molecular-dynamics (MD) simulations of the structure and dynamics of the 2D alkali-metal intercalate liquid became available, which have a direct bearing on the present QENS results as well as on complementary measurements of the intercalate in-plane phonon density of states determined by Kamitakahara and Zabel.²⁶ Ignoring the periodic potential of the substrate, White and Wielopolski²⁷ obtained from their MD simulation a dynamical structure factor $S(Q, \omega)$ which contains a central quasielastic component and a broad peak at finite ω , indicative of the existence of propagating density waves. These phononlike modes are, however, limited to Q values within the first diffuse liquid ring. This result is not too surprising and has also been obtained experimentally and theoretically for simple 3D liquids.^{28,29} In their recent molecular-dynamics simulation, Fan *et al.*³⁰ have taken the modulation potential explicitly into account. Their results not only show astounding agreement with the experimental liquid structure factor in stage-2 compounds, but also a dynamical structure factor which agrees extremely well with the inelastic-neutron-scattering data presented later in this paper.

In the past there have been several attempts to calculate the self-diffusion constant of intercalate atoms in graphite. DiVincenzo and Mele³¹ derived from a Thomas-Fermi density-functional calculation potential heights for various diffusion paths in stage 1 compounds. Thompson *et al.*³² and Moss *et al.*³³ have evaluated the modulation potentials from a crystallographic analysis of the alkali-metal contribution to the graphite *HKL* reflections in stage-2 KC_{24} and RbC_{24} compounds. Both the calculations of DiVincenzo and Mele³¹ and the x-ray determination of the substrate modulation potential^{32,33} are in close agreement with activation energies evaluated from the present diffusivity data. The MD simulations of Fan *et al.*³⁰ on RbC_{24} are particularly remarkable because of their excellent quantitative agreement with the experimental results.

The QENS studies described below are the first of its kind on graphite intercalation compounds. Short reports of this work have been published previously at several places.³⁴⁻³⁸ A complementary investigation of the in-plane vibrational dynamics of various stage-1 and -2 alkali-metal GIC's has been reported by Kamitakahara and Zabel.²⁶ The conclusions of that work will be tied in with the present QENS studies in Sec. V. In Sec. II we briefly review the experimental and theoretical method of QENS, in Sec. III we describe details of the experimental procedure, and in Sec. IV the experimental results are presented.

II. THEORETICAL BACKGROUND

Detailed reviews on the principles of QENS have been presented in Refs. 2–4 and are summarized by Magerl in Ref. 11. The purpose of the present section is therefore to outline only those aspects of the theory of QENS which are of immediate interest for the understanding and interpretation of the remainder of this paper.

The double-differential cross section for coherent and incoherent neutron scattering can be written³⁹

$$\left(\frac{d^2\sigma}{d\Omega dE'} \right)_{\text{coh}} = \frac{\sigma_{\text{coh}}}{4\pi} \frac{k'}{k} N S_{\text{coh}}(\mathbf{Q}, \omega), \quad (1)$$

$$\left(\frac{d^2\sigma}{d\Omega dE'} \right)_{\text{inc}} = \frac{\sigma_{\text{inc}}}{4\pi} \frac{k'}{k} N S_{\text{inc}}(\mathbf{Q}, \omega).$$

Here the subscripts coh and inc are abbreviations for coherent and incoherent, E' is the final neutron energy, k and k' are the initial and final neutron wave numbers, respectively, N is the total number of particles in the target, $\hbar\mathbf{Q} = \hbar(\mathbf{k}' - \mathbf{k})$ is the momentum transfer, and $\hbar\omega = E' - E$ is the energy change of the target. In the classical approximation the dynamical scattering function $S(\mathbf{Q}, \omega)$ represents the space and time Fourier transform of the self-correlation and pair correlation functions, $G_s(\mathbf{r}, t)$ and $G_p(\mathbf{r}, t)$, respectively,

$$S_{\text{coh}}(\mathbf{Q}, \omega) = \frac{1}{2\pi\hbar} \int [G_s(\mathbf{r}, t) + G_p(\mathbf{r}, t)] \times \exp[i(\mathbf{Q} \cdot \mathbf{r} - \omega t)] d\mathbf{r} dt, \quad (2)$$

$$S_{\text{inc}}(\mathbf{Q}, \omega) = \frac{1}{2\pi\hbar} \int G_s(\mathbf{r}, t) \exp[i(\mathbf{Q} \cdot \mathbf{r} - \omega t)] d\mathbf{r} dt.$$

The self-correlation function $G_s(\mathbf{r}, t)$ describes the time evolution of the spatial trajectory of a particular particle, while the pair correlation function $G_p(\mathbf{r}, t)$ represents the time and space correlation of two distinct particles.

In most QENS experiments reported in the past, only the incoherent scattering law has been investigated, for which relatively simple predictions exist for particle motions in ideal gases, liquids, or on well-defined lattice sites. This preference is furthermore supported by the availability of a very large incoherent scattering cross section for protons which is about 80 b, whereas the largest available coherent scattering cross section is smaller by roughly an order of magnitude. Thus, the bulk of QENS studies carried out so far is devoted to the investigation of the diffusivity of hydrogen in metals, of hydrogen-containing molecules and of hydrogenated polymers.

Unfortunately, the alkali-metal atoms of interest here exhibit rather small and almost entirely coherent scattering cross sections. Only Li offers an appreciable incoherent cross section. The coherent and incoherent cross sections for the four alkali-metal atoms in question are listed in Table I, and are reproduced from Ref. 40.

The coherent QENS due to the correlated motion of diffusing particles is by far more complex than the incoherent scattering from single-particle motion. Therefore only approximate expressions for the coherent

TABLE I. Coherent and incoherent cross sections for alkali-metal atoms. From Ref. 40.

Element	σ_{coh} (10^{-24} cm ²)	σ_{inc} (10^{-24} cm ²)
Li	0.45	0.91
⁷ Li	0.62	0.78
K	1.73	0.25
Rb	6.30	0.3
Cs	3.69	0.21

dynamical scattering function exist. The most successful prescription was given by Sköld,⁴¹ which relates the coherent scattering function to the incoherent one:

$$S_{\text{coh}}(\mathbf{Q}, \omega) = S(\mathbf{Q}) S_{\text{inc}}(\mathbf{Q}/\sqrt{S(\mathbf{Q})}, \omega), \quad (3)$$

where the zeroth energy moment is the structure factor:

$$S(\mathbf{Q}) = \int S_{\text{coh}}(\mathbf{Q}, \omega) d\omega. \quad (4)$$

For reference, in subsequent sections we will give the scattering functions for continuous liquidlike diffusion and for a lattice-gas hopping motion. Using a Gaussian approximation for the spatial part of the self-correlation function, the incoherent dynamical scattering function becomes

$$S_{\text{inc}}(\mathbf{Q}, \omega) = \frac{1}{\pi\hbar} \frac{DQ^2}{(DQ^2)^2 + \omega^2}, \quad (5)$$

which has a Lorentzian shape and a full width at half maximum (FWHM):

$$\Gamma_{\text{inc}} = 2\hbar DQ^2. \quad (6)$$

Therefore, the quasielastic linewidth increases quadratically with the scattering vector Q and is proportional to the self-diffusion constant D . Using the scaling relation of Eq. (3), we obtain for the width of the coherent dynamical scattering function

$$\Gamma_{\text{coh}} = \frac{\Gamma_{\text{inc}}}{S(\mathbf{Q})}. \quad (7)$$

Thus, for coherently scattering particles the linewidth scales with the static structure factor and exhibits characteristic de Gennes oscillations according to the oscillations of $S(\mathbf{Q})$. These de Gennes oscillations are schematically shown in Fig. 1 for the case of a simple continuous liquidlike diffusion process. The minima of Γ_{coh} occur at positions of \mathbf{Q} for which $S(\mathbf{Q})$ has maxima, i.e., for wave vectors which correspond to most probable interatomic distances in the liquid. These distances are due to highly correlated atomic configurations and are long lived because of the cooperative motions necessary to break them up. This long lifetime is then reflected as a narrowing in the linewidth Γ_{coh} for those wave vectors. For larger Q values, $S(\mathbf{Q})$ approximates the constant value of 1, reflecting the loss of correlation over very small distances. In this approximation, the single-particle picture is again valid, and $\Gamma_{\text{coh}}(\mathbf{Q}) = \Gamma_{\text{inc}}(\mathbf{Q})$.

In high-resolution QENS experiments using long-

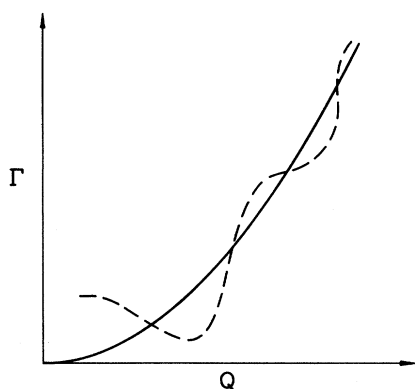


FIG. 1. Schematics of the quasielastic linewidth Γ plotted as a function of the scattering vector Q for simple liquidlike diffusion. The solid line represents the width for incoherently scattering particles, $\Gamma_{\text{inc}} = 2\hbar DQ^2$, while the dashed line is the quasielastic linewidth expected from coherently scattering particles. The oscillation of the Γ_{coh} is caused by coherency effects of the liquid structure factor and is often referred to as the de Gennes oscillation.

In high-resolution QENS experiments using long-wavelength neutrons, the limit $S(Q) \rightarrow 1$ usually cannot be reached. Diffusion constants can, nevertheless, be extracted from coherent quasielastic neutron scattering data, most conveniently at positions for which $S(Q)$ passes through 1. For those Q values, Eq. (6) is again valid, and from an Arrhenius plot of the diffusion constant

$$D = D_0 e^{-E_a/k_B T}, \quad (8)$$

the activation energy E_a for the self-diffusivity and the prefactor D_0 can be determined.

For jumplike particle motions instead of continuously moving particles, again, a Lorentzian-shaped incoherent scattering function is obtained, whose width

$$\Gamma_{\text{inc}} = 2\hbar f(Q)/\tau \quad (9)$$

depends on the mean residence time τ between the jumps and a model-dependent geometric width function:

$$f(Q) = \frac{1}{n} \sum_{i=1}^n [1 - \exp(-i\mathbf{Q} \cdot \mathbf{l}_i)]. \quad (10)$$

Here, \mathbf{l}_i is the jump vector and the sum is taken over all possible neighbor sites at distance $|\mathbf{l}_i|$ from the particle. Γ_{inc} for jump diffusion exhibits an oscillatory Q dependence with nodes at $|\mathbf{Q}| = 2\pi/|\mathbf{l}|$ in a single-crystal situation. For powders a proper angular average has to be carried out, but characteristic dips in $\Gamma_{\text{inc}}(Q)$ remain, from which the jump vectors can be determined. These oscillations have to be distinguished from the de Gennes oscillations. The former occur in the incoherent scattering function due to the presence of discrete jump vectors, while the latter are present in the coherent scattering function even for a continuously diffusing particle, because of the oscillation of the structure factor $S(Q)$.

It should be noted that the connection between diffusion constants and jump vectors in two dimensions is given by

$$D = l^2/4\tau, \quad (11)$$

independent of the number of nearest-neighbor sites in the plane, whereas in three dimensions the diffusion constant is given by

$$D = l^2/6\tau. \quad (12)$$

III. EXPERIMENT

In the present experiments on K, Rb, and Cs intercalation compounds, we used pyrolytic graphite with a starting crystal mosaic nature of about 6° – 8° . The pristine graphite material was cut to cylindrically shaped disks of 18–22 mm diameter and stacked together to a height of 40–50 mm. Intercalation was achieved by the usual two-zone vapor-phase technique and by using natural isotropic mixtures of K, Rb, and Cs from A.D. Mackay with a stated purity of 99.9%. After intercalation, the stage purity was determined by (00 l) x-ray and neutron scans, and only high-quality samples were used for subsequent QENS experiments. The samples were finally taken out of the glass container in which they were intercalated and transferred into thin-walled Al sample chambers inside of a high-purity He glove box. The sample cans were compression-sealed with a tapered stainless-steel cap, which provided a good seal at low and high temperatures. The schematic of the sample chamber used is shown in Fig. 2. To avoid a possible leakage of alkali metals through the Al walls at high temperatures, we used thin-walled stainless-steel cans instead, which were sealed by Cu caps for measurements above 600 K.

The LiC_6 sample was prepared in a different way. Pyrolytic graphite, with a 3° mosaic spread, was sliced into disks of about 1 mm thickness and 40 mm diameter. The slices were then completely immersed in liquid lithium and heated to 300°C for about 4 weeks in an evacuated stainless-steel crucible. Instead of using a natural isotropic mixture of Li metal, we used 97% enriched ^7Li from Oak Ridge National Laboratory. This was done to reduce the neutron-absorption cross section in the large sample. After completion of the intercalation process, which could visually be monitored by a bright and homogeneous golden color of the sample, any excess Li on the surfaces was cleaned off and the disks were placed in a thin-walled stainless-steel container suitable for neutron scattering. The sample can was also filled with about 2–3 g of ^7Li metal at the bottom, separated from the intercalated sample by a perforated platform and shielded from the neutron beam by a Gd foil. This assembly allowed the study of the diffusivity of Li atoms in LiC_6 at high temperatures without deintercalating the compound.

The LiC_6 sample had a volume of 31 cm^3 , whereas all other stage-1 and -2 compounds had volumes ranging from 10 to 15 cm^3 . The LiC_6 sample was used previously for the measurement of the phonon dispersion;⁴² all other

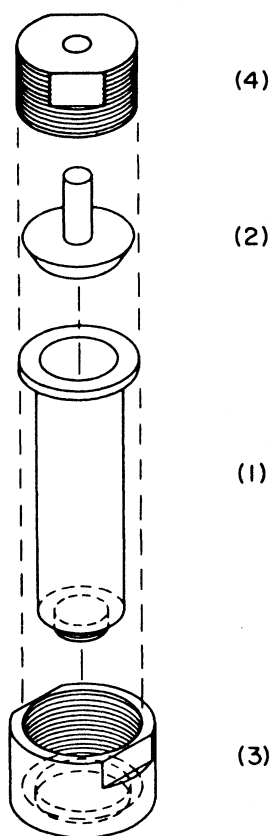


FIG. 2. Sample chamber for neutron scattering work. (1) Thin-walled cylindrical aluminum can. (2) Stainless-steel cone. (3) and (4) Stainless-steel screw and nut for pressing the cone on the Al inside edge.

samples were prepared specifically for the present diffusion studies.

The neutron scattering experiments were carried out using the time-of-flight (TOF) spectrometers IN5 and IN6 and the backscattering spectrometer IN10 of the Institut-Laue-Langevin. All three instruments are located at the cold-neutron source within the neutron guide hall. For general descriptions and specifications of the spectrometers, we refer to the user manual of the Institut-Laue-Langevin.⁴³ The specific conditions of our operation of the spectrometers will be stated later in the next section. In most of our scattering experiments the c axis was aligned perpendicular to the scattering plane, in which case the diffusional motion of the alkali-metal atoms parallel to the intercalate plane is studied. In only a few cases we have tilted the c axis into the scattering plane for testing the possibility of diffusion through the graphite basal planes.

For each experimental configuration we have determined the instrumental shape function and the background scattering, and we have used vanadium standards for converting count rates into absolute dynamical scattering functions.

IV. EXPERIMENTAL RESULTS

In this section we will first discuss stage-1 compounds which exhibit commensurate superstructures in their ordered phases. Because of the relatively large metal-substrate interaction, 2D lattice liquid jump diffusivities are expected for these compounds. Stage-2 compounds, to be discussed next, are very different from stage-1 compounds, as detailed in the Introduction. The average in-plane density of the intercalate layers is lower and the structure has to be understood in terms of competing metal-metal and metal-substrate interactions. Accordingly, we expect the diffusional dynamics of the alkali-metal atoms in stage-2 compounds to be, by far, more complex than in stage-1 compounds.

A. LiC_6

The intercalate layers in LiC_6 form a $(\sqrt{3} \times \sqrt{3})R 30^\circ$ superstructure, which melts at 715 K.^{44,45} The order-disorder phase transition appears to be almost second order with a small first-order-type jump in the order parameter, and the transition temperature was shown to depend sensitively on the in-plane concentration.⁴⁶ The $(\sqrt{3} \times \sqrt{3})R 30^\circ$ structure has three equivalent sites; however, only one of them is occupied in the ordered state, resulting in a stacking sequence $A\alpha A\alpha A\alpha\dots$ of the graphite and intercalate layers. Therefore, all layers are aligned on top of each other, and the Li atoms in graphite may be viewed as forming chains along the c axis. This, and the small separation of the graphite layers in LiC_6 , which is only 3.71 Å, as compared to 3.35 Å for pristine graphite, may be taken as an indication for the existence of large-amplitude fluctuations or even diffusion of the Li atoms through the carbon hexagon rings provided by the graphite basal-plane structure.

For neutron scattering, $^7\text{LiC}_6$ is quite unique among the GIC's. The isotope ^7Li is the only alkali metal that exhibits an appreciable spin-incoherent cross section of 0.7 b (see Table I) along with a negligible neutron-absorption cross section. The incoherent cross section enables the exploration of the Li diffusivity both in the ordered as well as in the disordered phase, while the small absorption cross section allows one to compensate for the small scattering cross section by a large sample size.

In the ordered phase of LiC_6 the coherent scattering cross section is almost entirely concentrated in the Bragg peaks of the superstructure, whereas the incoherent contribution forms a featureless background. Above the disordering temperature the Li intercalate layers presumably exhibit a lattice LSF,⁴⁷ consisting of Bragg reflections at the $HK0$ reciprocal-lattice points of the graphite basal-plane structure superimposed on short-range-order diffuse intensity. The incoherent scattering contribution is unaffected by the phase transition. Neglecting all pair correlations, we can approximate the coherent diffuse contribution by the Laue expression $c(1-c)Nb_{\text{coh}}^2$, where $c = \frac{1}{3}$ is the ratio of occupied to available lattice sites in the disordered state, and the incoherent scattering contribution is simply given by Nb_{inc}^2 .

Therefore, we estimate that the ratio of the incoherent to the coherent scattering away from Bragg reflections and above T_c is on the order of 7. From this we can conclude that above as well as below the transition temperature the QENS signal from diffusion of ^7Li is dominated by the incoherent scattering function.

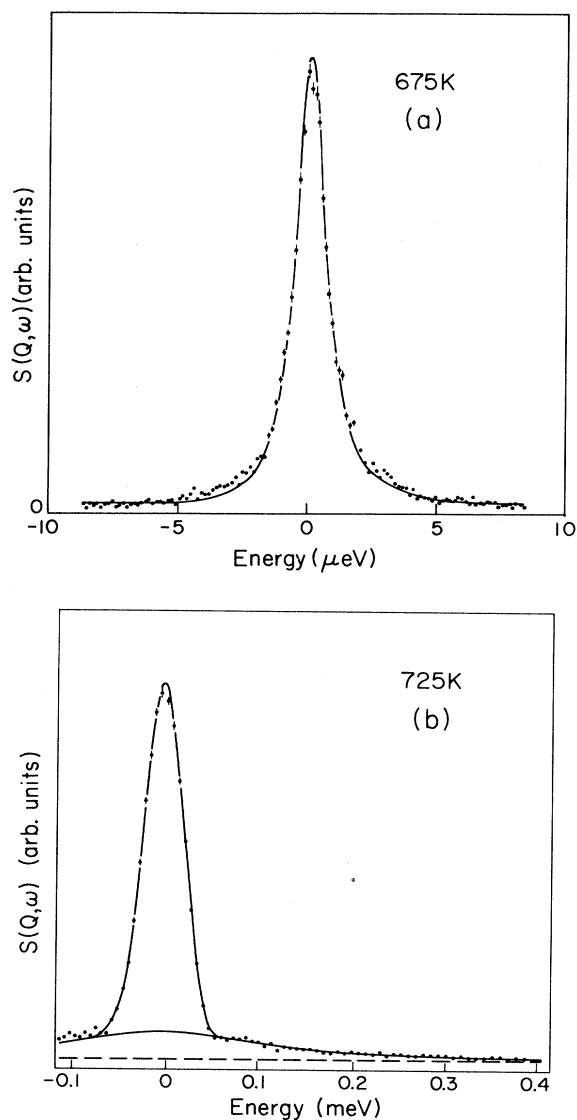
QENS measurements from below the ordering temperature up to 725 K were carried out at the backscattering spectrometer IN10 with a neutron wavelength of 6.28 Å and an energy resolution of 1.0 μeV . The much enhanced diffusivity of the Li atoms in the disordered state demanded the use of a lower-resolution instrument. Data above T_c were therefore recorded on the TOF spectrometer IN5 with a resolution of 63 μeV .

Typical quasielastic spectra taken on the TOF spectrometers IN5 and IN10 are reproduced in Fig. 3. The quasielastic Lorentzian component is shown by thin solid lines, representing only a small fraction of the total scattering. The dominant contribution to the scattering is elastic and temperature independent and appears to originate from the stainless-steel sample container. The low-temperature IN5 data show no quasielastic broadening and thus merely reflect the resolution of the spectrometer. With the higher resolution IN10 backscattering spectrometer, the diffusivity becomes noticeable already at 625 K, or 90 K below the melting temperature. Above the melting temperature the width increases dramatically and the Lorentzian peak becomes indistinguishable from a background within the dynamical range of this instrument. At this point a lower-resolution spectrometer, the TOF IN5, is required to refocus on the quasielastic line shape. In order to avoid the formation of Li_2C_2 , the sample was not heated above 725 K.

We have also investigated the possibility of an out-of-plane diffusive motion of the Li ions. In scans up to 675 K we have not noticed any quasielastic broadening of the dynamical scattering function, setting an upper limit for the diffusion constant along the channels in the hexagonal direction, which, according to the resolution of the instrument, is $D < 10^{-8} \text{ cm}^2/\text{sec}$.

All spectra were fitted with a constant background, a δ function, and one Lorentzian line shape, convoluted with the instrumental width function. The Q dependence of Γ_{inc} as determined from the full width at half maximum (FWHM) of the Lorentzian component is shown in Fig. 4 for two temperatures above and below the melting temperature. At 660 K, 55 K below the melting transition, Γ_{inc} increases to a maximum of 4 μeV at $Q \cong 1.0 \text{ \AA}^{-1}$, followed by a decrease for higher Q values. This in contrast to the Q dependence of Γ_{inc} above T_c , where Γ_{inc} reaches a maximum of 230 μeV at a higher Q value of 1.4 Å^{-1} . The oscillatory behavior of Γ_{inc} immediately reveals a jumplike diffusivity of the Li intercalate ions at both temperatures. Moreover, the shift of the maximum from a lower value below the melting temperature to a higher value above the melting temperature indicates that the jump vector decreased in magnitude upon crossing the melting temperature.

The structure of LiC_6 is suggestive for two possible jump vectors sketched in the inset of Fig. 4: those may be either jumps to nearest hexagon centers with a jump



the scattering vector oriented parallel to the intercalate planes. (a) $S(Q, \omega)$ measured with the backscattering spectrometer IN10 at $Q = 1.4 \text{ \AA}^{-1}$ and 675 K. The solid line represents a fit by a δ function convoluted with the instrumental resolution function. The extra scattering in the wings is attributed to quasielastic scattering from planar Li diffusion. (b) $S(Q, \omega)$ measured with the time-of-flight spectrometer IN5 at $Q = 1.125 \text{ \AA}^{-1}$ and at 725 K. The solid line through the data points represents a best fit by a δ function and a Lorentzian function both convoluted with the instrumental resolution function. The lower solid line shows the Lorentzian contribution alone.

length $l_1 = 2.46 \text{ \AA}$, or jumps to next-nearest hexagon centers at a distance $l_2 = 4.26 \text{ \AA}$, connecting sites within the same superstructure. For a single-crystal situation and for scanning along the [100] direction, one obtains from Eq. (10) the following Q dependence for the quasielastic broadening:

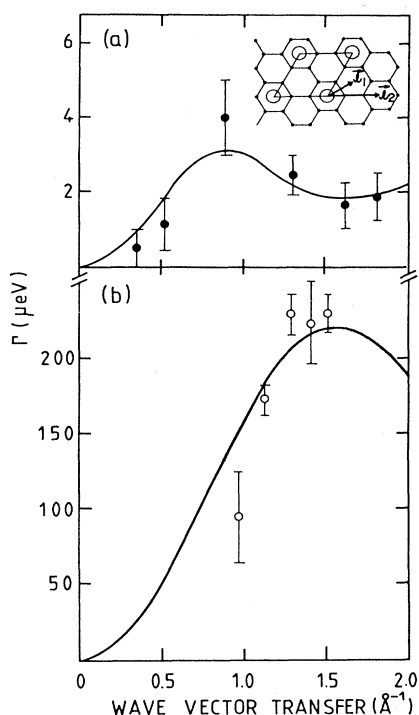


FIG. 4. Linewidth of quasielastic neutron spectra measured as a function of the scattering vector Q parallel to the intercalate layers in LiC_6 for temperatures (a) 660 K and (b) 720 K. The linewidths in (a) are recorded below, and in (b) just above, the melting temperature of the Li sublattice at the 715 transition of the Li sublattice. The inset shows the $(\sqrt{3} \times \sqrt{3})R 30^\circ$ superstructure in the ordered phase together with possible jump vectors l_1 to nearest-neighbor sites and l_2 to next-nearest-neighbor sites. The solid lines are best fits of Eq. (14) to the data points, indicating that below T_c a jump vector l_2 predominates which connects sites within the same sublattice, while above T_c also jumps to nearest-neighbor sites (l_1) become available.

$$\Gamma_{\text{inc}} = \frac{4\hbar}{3\tau} \left[\sin^2 \left[\frac{Ql}{2} \right] + 2 \sin^2 \left[\frac{Ql}{4} \right] \right], \quad (13)$$

where l may be either l_1 or l_2 . In our present situation of pyrolytic graphite, a proper 2D orientational average has to be carried out and we obtain

$$\Gamma_{\text{inc}} = \frac{2\hbar}{\tau} [1 - J_0(Ql)]. \quad (14)$$

Here, τ is the mean residence time and J_0 is the zeroth-order Bessel function.

In Fig. 4 the solid lines are fits of Eq. (14) to the data points assuming $l=l_2$ for $T < T_c$ and $l=l_1$ for $T > T_c$. Although the total Q range is limited due to the use of cold neutrons, the fits are strongly suggestive for a jump-like diffusion process in the ordered as well as in the disordered state. In addition, the data suggest a change in the jump distance upon crossing the melting transition. In the ordered phase diffusive jumps connect sites within the same sublattice of the $(\sqrt{3} \times \sqrt{3})R 30^\circ$ structure, whereas above T_c all three sites α , β , and γ become available as the Li atoms hop on the hexagonal graphite grid.

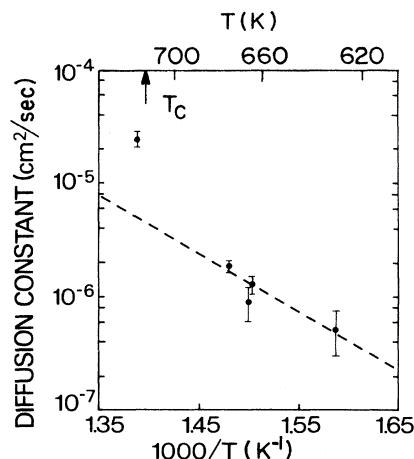


FIG. 5. Arrhenius plot for the diffusion constant of planar Li diffusion in the ordered phase of LiC_6 . The dashed line is a best fit to the data points with an activation energy of 1.0 eV. The single data point above the dashed line indicates the diffusion constant at 720 K in the disordered phase.

We have calculated diffusion constants from the absolute values of the quasielastic line broadening Γ_{inc} via Eq. (6), and those are shown in an Arrhenius plot in Fig. 5. For the ordered state we find an activation energy of $E_a = (1.0 \pm 0.3)$ eV. The rather large error bar is made up by the small incoherent signal and the limited number of temperature points evaluated below T_c . Above T_c a dramatic enhancement of the diffusivity takes place, indicating a decrease of the activation energy. We have, however, not extracted an activation energy for the disordered state because of the small temperature range over which we were able to measure the diffusivity without deteriorating the sample.

The present data compare favorably with diffusion measurements via the βNMR (or in-beam NMR) method applied by Heitjans and co-workers.⁴⁸ For the ordered phase from 250 to 700 K they have obtained an activation energy of (0.6 ± 0.2) eV, which is in rough agreement with our present results. An activation energy of only 0.2 eV was measured by Estrade *et al.*⁴⁹ using conventional NMR techniques, which clearly appears to be too small in the light of the present data.

DiVincenzo and Mele³¹ have calculated the potential barrier for Li diffusion in LiC_6 via a density-functional approach. Assuming that this barrier height is identical to the activation energy for a classical jumplike diffusion process, they obtain an activation energy of 1.3 eV, which is in rather close agreement with our experimental results.

The activation energy below T_c most likely contains contributions from the enthalpy of vacancy formation as well as from the potential barrier to the diffusion. If only the potential height for the diffusion were contributing to the measured activation energies, it would be difficult to understand why the diffusion constant suddenly increases above T_c . On the other hand, the agreement with the density-functional calculation of DiVincenzo and Mele is

TABLE II. Structural parameters.

Compound	Structure	Melting temperature		Reference
		T_L (K)	T_U (K)	
LiC ₈	$(\sqrt{3} \times \sqrt{3})R30^\circ$		715	44,45
KC ₈	$(2 \times 2)R0$	657	687	50 ^b
		677	682	53
		750	785	51 ^c
RbC ₈	$(2 \times 2)R0$	736	774	53
		721	747	52
		123		55,57
KC ₂₄	DDL ^a	165		28,58
RbC ₂₄	DDL ^a	165		56
CsC ₂₄	DDL ^a			

^aDDL denotes discommensuration domain lattice.

^bFrom phase diagram for the condition that free K metal and intercalate sample are at the same temperature.

^cFrom phase diagram for the condition that free Rb metal and intercalated sample are at the same temperature.

rather good, and these calculations did not take vacancy-formation energies into account. This conflict cannot be resolved here and should be made the subject of future investigations.

B. KC₈ and RbC₈

Both stage-1 compounds with K and Rb exhibit a $(2 \times 2)R0$ in-plane structure with a stacking sequence $A\alpha A\beta A\gamma A\delta A\alpha\dots$. The disordering of the alkali-metal layers occurs in two steps. A stacking disorder takes place at a lower transition temperature T_L and is followed by a disordering of the in-plane structure at higher temperatures T_U .^{50,51} These phase transitions have been studied in detail by a number of workers⁵⁰⁻⁵⁴ using a variety of methods, and the transition temperatures from those investigations are listed in Table II.

As mentioned before, the exploration of the diffusion mechanism in the ordered phases of KC₈ and Rb₈ is hampered by the fact that both alkali-metal atoms exhibit almost completely coherent scattering cross sections. QENS experiments of these compounds can therefore be carried out only in their disordered states. The experiments were performed with the TOF spectrometer IN6 and with a wavelength of 5.1 Å, yielding a resolution of about 70 μeV.

The Q dependence of the quasielastic linewidth Γ_{coh} for KC₈ is shown in Fig. 6 for the temperatures 623 and 698 K. Both temperatures appear to be above the melting temperature. This conclusion follows from the structure factor $S(Q)$, which is reproduced for 623 K in the bottom panel of Fig. 6. $S(Q)$ has been obtained by energy integration of the Lorentzian part of the energy spectrum. The first maximum in the structure factor occurs at 1.4 Å⁻¹ and has a width of $\Delta Q \cong 0.4$ Å⁻¹. The position as well as the width of this peak are clear signatures of a "liquidlike" state of the intercalate layers, and are in excellent agreement with the x-ray work of Minemoto and Suematsu.⁵⁰ Considering that any excess alkali metal in the sample container produces an alkali-metal vapor pressure corresponding to the sample temperature, an

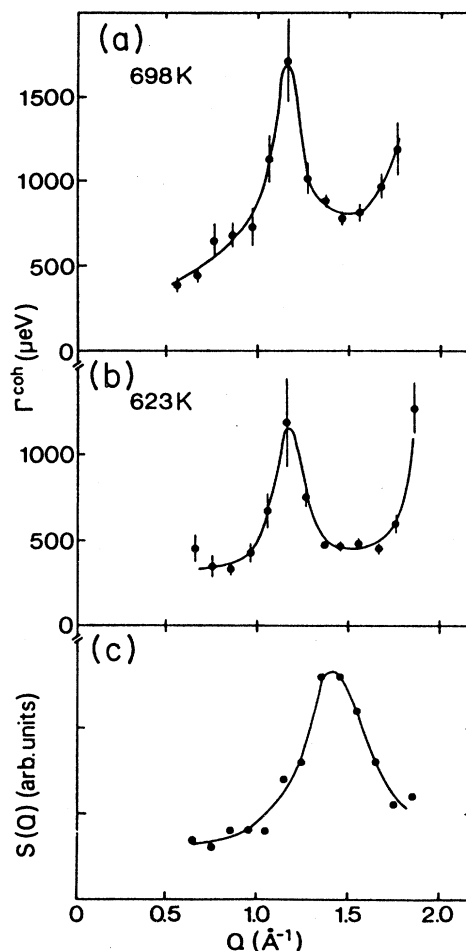


FIG. 6. Quasielastic width as a function of the scattering vector Q for K diffusion in KC₈ (a) at 698 K and (b) at 623 K. (c) Structure factor $S(Q)$ for the disordered alkali-metal layer obtained from integrating the Lorentzian line shape at 623 K.

order-disorder transition of about 650 K can be inferred from the phase diagram of Minemoto and Suematsu,⁵⁰ which is somewhat higher than the transition temperature observed here.

For both temperatures shown in Fig. 6 the quasielastic linewidths exhibit a pronounced structure. Γ_{coh} exhibits a maximum at about 1.15 \AA^{-1} and a minimum at 1.5 \AA^{-1} . The minimum coincides with the first maximum of the alkali-metal intercalate LSF shown in the bottom panel, confirming that the dip in the quasielastic width at $Q = 1.5 \text{ \AA}^{-1}$ is due to a de Gennes narrowing effect rather than discrete jump vectors. Although we believe that the diffusion motion in KC_8 is almost certainly of the jump type, as in LiC_6 , it is very difficult to obtain a precise microscopic picture because of the interfering coherency effects.

The spectra reveal, nevertheless, important information on the diffusion constant. At positions where $S(Q)$ is approximately 1, the coherent and incoherent linewidths are identical and the diffusion constant can be evaluated at those point. Although an evaluation of $S(Q)$ in absolute units could not be achieved because of the lack of high- Q data, a reasonable guess can be made toward the Q value at which $S(Q)$ passes through 1. Referring to Fig. 6, we argue that $S(Q) \cong 1$ at about $Q = 1.1 \text{ \AA}^{-1}$. Using the values for Γ_{coh} at this Q point, we obtain the diffusion constants $D = 5.6 \times 10^{-5}$ and $8.1 \times 10^{-5} \text{ cm}^2/\text{sec}$ for the temperatures 623 and 698 K, respectively, which, in turn, yields an activation energy of $E_a = 0.18 \text{ eV}$.

The activation energy for K diffusion in KC_8 is considerably smaller than for the diffusion of Li ions in LiC_6 . This is not unexpected, since both the larger separation of graphite planes and the lower melting temperature point to a weaker interaction of the potassium ions with the graphite substrate. According to DiVincenzo and Mele,³¹ the activation energy is again given by the classical potential barrier which stretches between the C—C bonds, and for which they obtain a value in exact agreement with our experimental data (see Table III).

We now turn to a discussion of RbC_8 . In order to monitor the order parameter of RbC_8 , we measured $S(Q, \omega=0)$ at $Q = 1.5 \text{ \AA}^{-1}$ using the TOF spectrometer

IN6. The sample chamber contained some excess Rb metal at the bottom separated from the sample by a perforated platform. This extra metal fulfilled the purpose of keeping the free and intercalated alkali metal in thermodynamic equilibrium while being at the same temperature. The temperature dependence of $S(1.5, 0)$ measured under those conditions is shown in Fig. 7. Here, $\omega=0$ refers to an energy window of $\Delta\omega = 70 \text{ \mu eV}$ given by the instrumental resolution. $S(1.5, 0)$ exhibits a first dip at 650 K, reaches a plateau between 670 and 740 K, and drops to a background level at 780 K. The phase diagram of RbC_8 (Ref. 51) indicates for the conditions realized here a stacking transition $\alpha\beta\gamma\delta \rightarrow \alpha\beta$ at $T_1 = 750 \text{ K}$ and an order-disorder transition at $T_u = 785 \text{ K}$. The $S(Q, 0)$ data compare well with the upper phase transition, while the reason for the intensity drop at 650 K is not obvious from the phase diagram.

Quasielastic broadening of the scattering function is clearly observable between 700 and 780 K with an onset at 750 K. This corresponds to a temperature below T_u where the order parameter of the ordered $(2 \times 2)R0$ structure is reduced but not vanished (compare Fig. 7). A quantitative analysis for these spectra has not been carried out. The spectra demonstrate, however, that the onset of the alkali-metal intercalate diffusion can be observed before the structural order parameter reaches zero, which again is a clear sign for a vacancy-controlled diffusion mechanism, much like in LiC_6 below the order-disorder transition.

C. KC_{24} , RbC_{24} , and CsC_{24}

1. Structure

A comprehensive review of the structural studies of stage-2 alkali-metal compounds has recently been provided by Moss and Moret⁷ and shall briefly be summarized here. There is general agreement that above the intercalate ordering transitions the intercalate "liquidlike" structure factor exhibits pure 2D correlations and is anisotropic within the plane due to the modulation effect of the sixfold graphite substrate potential. Quotation marks are used around the term "liquidlike" because, from a structural point of view, a liquid and an amorphous state

TABLE III. Diffusion constants and activation energies for intercalate alkali-metal atoms in graphite.

Compound	D_0 (cm^2/sec)	E_a (eV)	Barrier height (eV)
LiC_6	51	1.0	1.3 ^a
KC_8	16.0×10^{-4}	0.18	0.18 ^a
RbC_8			0.14 ^a
CsC_8			0.18 ^a
KC_{24}	1.2×10^{-4}	0.126	
RbC_{24}	2.5×10^{-4}	0.063	0.092 ^b
CsC_{24}	4.3×10^{-4}	0.077	

^aFrom DiVincenzo and Mele, Ref. 31.

^bFrom Moss *et al.* Ref. 33.

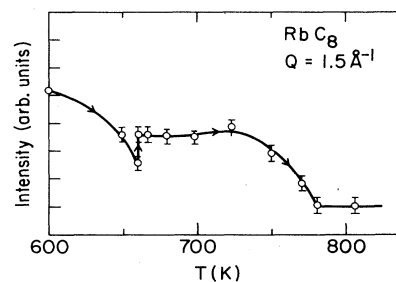


FIG. 7. Temperature dependence of the elastic structure factor of RbC_8 at the scattering vector $Q = 1.5 \text{ \AA}^{-1}$ pointing parallel to the intercalate layers.

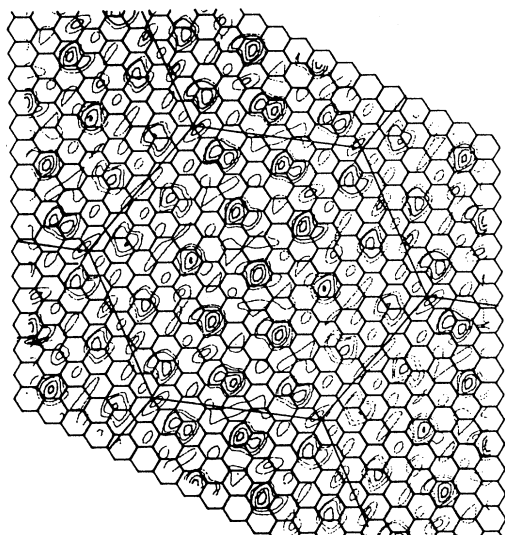


FIG. 8. Density-contour map for alkali-metal atoms in stage-2 CsC_{24} , obtained from Fourier backtransformation of low-order intercalate superstructure reflection intensities. The solid lines are idealized domain walls and serve as a guide to the eye. At the center of the domains the alkali-metal atoms assume registered positions with the graphite honeycomb structure forming $(\sqrt{7} \times \sqrt{7})R19.1^\circ$ structures whereas closer to the domain walls deviations from commensurate sites occur.

cannot be distinguished, the main difference between them being their varying dynamical response. At the in-plane ordering temperatures T_c , which are listed in Table II for the three stage-2 compounds, a 2D-3D crossover effect of the intercalate correlation takes place. Below T_c the diffraction pattern is that of two incommensurate and modulated lattices, the host and the guest lattice. The interpretation of the diffraction pattern has seen many stages. A highly plausible model, which successfully describes the most important features of the diffraction pattern, is the discommensuration domain model.⁵⁹⁻⁶¹ According to this model, the alkali-metal atoms order in an array of large domains, which are slightly rotated against the graphite symmetry axis. Near the domain centers the intercalate atoms are well registered in a $(\sqrt{7} \times \sqrt{7})R19.1^\circ$ lattice, while the atoms near the domain walls show deviations from registry with the graphite hexagon centers and are more spread out. A real-space density-contour map of the atoms in the discommensurate domain lattice is reproduced in Fig. 8. The rotation angle and the domain size are intimately related to each other and are shown in Fig. 8 for the case of CsC_{24} . The structural inequivalency of atoms sitting close to the centers as compared to those situated near domain walls has important implications for the dynamics of the alkali-metal atoms, as we will discuss further below.

2. Temperature dependence of quasielastic spectra

Quasielastic spectra for the three stage-2 compounds MC_{24} ($M = \text{K}, \text{Rb}, \text{and Cs}$) have been recorded using the

TOF spectrometer IN6 with a neutron wavelength of 5.1 Å and an energy resolution of 100 μeV .

With the present instrumental resolution, the Lorentzian broadening of the scattering function first becomes noticeable above the ordering temperatures of the stage-2 compounds. Most importantly, this Lorentzian broadening does not immediately affect the total scattering function, but only part of it. A typical example is reproduced in Fig. 9, which shows the dynamical scattering function for RbC_{24} at 236 and 343 K and at scattering vector $Q = 1.25 \text{ \AA}^{-1}$. The solid line represents a fit with a δ function and a Lorentzian line shape both convoluted with the instrumental width function. The dashed line indicates only the Lorentzian contribution. Note that the Lorentzian part broadens as well as increases in intensity with increasing temperature. This behavior reveals clear signs, first for a speeding up of the particles with increasing temperature, and second for an increase of the number of particles taking part in the diffusion process. While the first behavior is normal, the second represents a novel feature of this two-dimensional melting transi-

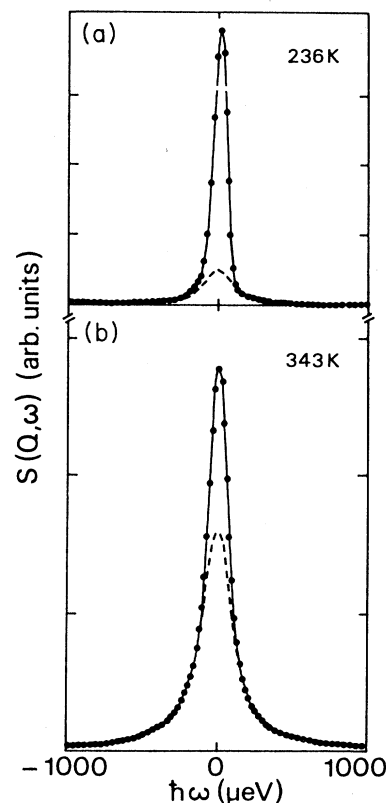


FIG. 9. Dynamical scattering function $S(Q, \omega)$ of RbC_{24} as a function of ω at $Q = 1.25 \text{ \AA}^{-1}$ measured at (a) 236 K and (b) 343 K. The solid lines represent fits of a δ function and a Lorentzian line shape, both convoluted with the instrumental width function to the data points (solid dots). The dashed line shows only the Lorentzian part of the total scattering function. Note that this Lorentzian contribution increases with increasing temperature.

tion. Therefore, we have to conclude that there are two types of alkali-metal atoms within the same intercalate gallery. Those which exhibit diffusive motion are represented by a Lorentzian line shape, while the more rigid atoms are represented by the δ -function.

We have calculated the partial structure factors $S_\delta(Q)$ and $S_L(Q)$ by integrating independently over the δ and the Lorentzian components:

$$\begin{aligned} S_\delta(Q) &= \int S_{\text{coh}}^\delta(Q, \omega) d\omega, \\ S_L(Q) &= \int S_{\text{coh}}^L(Q, \omega) d\omega. \end{aligned} \quad (15)$$

The integration was carried out within the limits $-1 \leq \omega \leq 1$ meV and for Q values between 0.75 and 2.2 \AA^{-1} . The partial structure factors for RbC_{24} are shown in Fig. 10 at two different temperatures above the ordering transition. The startling result of this figure is that both partial structure factors are topologically similar and that they conform to the total "liquidlike" structure factor $S(Q) = S_{\text{coh}}^\delta(Q) + S_{\text{coh}}^L(Q)$ as measured by x-ray scattering.⁶² Therefore both scattering components originate from the 2D alkali-metal layers and reflect the disorder of the intercalate structure at these temperatures. Furthermore, Fig. 10 reveals a tradeoff between the δ and the Lorentzian part of the structure factors. Therefore, above T_c the solid and liquidlike dynamical behaviors

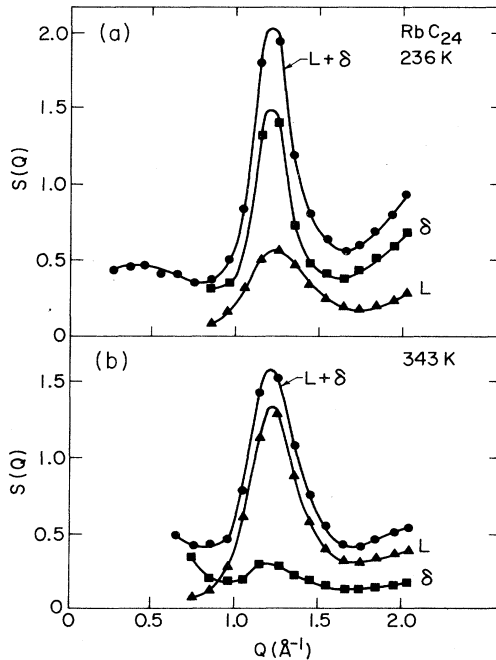


FIG. 10. Partial structure factors $S_\delta(Q)$ and $S_L(Q)$ of RbC_{24} from independent energy integrations of the δ part and the Lorentzian (L) part of the dynamical structure factor, and for two temperatures: (a) 236 K and (b) 343 K. The solid line marked $L + \delta$ represents the sum of both components and is identical to the total structure factor usually measured in x-ray scattering experiments.

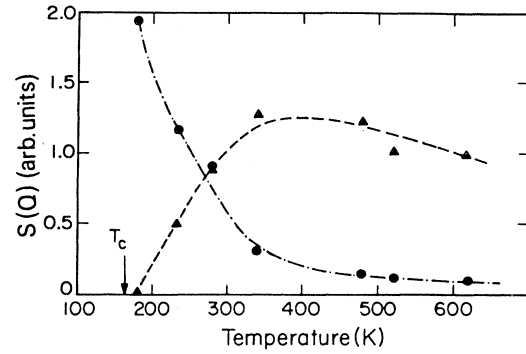


FIG. 11. Temperature dependence of the structure factors $S_\delta(Q)$ and $S_L(Q)$ of RbC_{24} at $Q = 1.20 \text{ \AA}^{-1}$. The arrow indicates the critical temperature for the melting transition in RbC_{24} at 165 K.

coexist and their relative weights gradually exchange with increasing temperature. This is shown clearly in Fig. 11, where the values of $S_{\text{coh}}^\delta(Q)$ and $S_{\text{coh}}^L(Q)$ at $Q = 1.2 \text{ \AA}^{-1}$ are plotted as a function of temperature. The Lorentzian contribution to the intensity smoothly increases from $T_c = 165$ –350 K, or about 200 K above the melting transition, and then levels off. The slight decrease of the intensity is likely due to Debye-Waller-factor effects. Simultaneously, the δ component decreases slowly over the same temperature range.

The coexistence of a solidlike elastic and liquidlike diffusive dynamical structure factor $S(Q, \omega)$ in thermal equilibrium and over a wide temperature range above the structural melting transition is an entirely new phenomenon not known for simple 3D systems. In 3D monatomic liquids, a δ -like component in $S(Q, \omega)$ does not exist for any temperature above the melting temperature. We believe that the dynamical behavior observed here is characteristic for the melting of a 2D monatomic layer on a periodic substrate. In our view the melting starts first at the domain walls, effectively unpinning the commensuration domain boundaries. The domains are then free to float, and it has been shown that this causes the layer shear elastic constant to become extremely soft.³⁷ The meandering of the domain walls and the oscillation of the domain sizes may then be the source for the quasielastic broadening of the structure factor. However, at the center of the freely floating domains the effect of the substrate potential is still strong enough to produce an elastic component in the dynamical structure factor $S(Q, \omega)$.

3. Q dependence of Γ_{coh}

The Q dependence of the quasielastic linewidths for RbC_{24} and for several temperatures is reproduced in Fig. 12. The salient features of this figure are (i) the width of the spectra increases with increasing temperature, (ii) the Q dependence of Γ_{coh} exhibits de Gennes narrowing effects, and (iii) this narrowing coincides with the maximum in the intercalate liquid structure factor, which

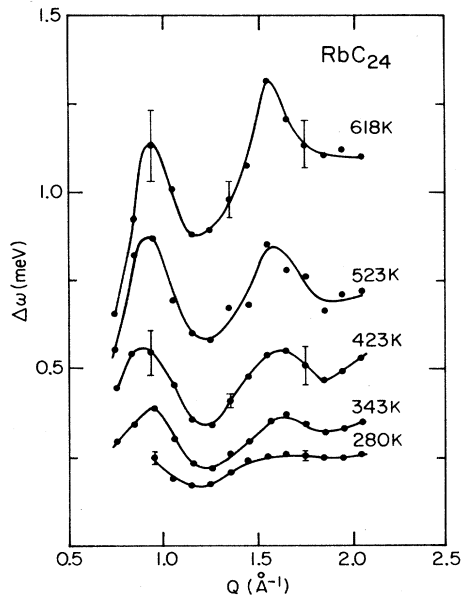


FIG. 12. Energy widths of the Lorentzian component of the dynamical scattering function $S(Q, \omega)$ with dependence on the scattering vector Q and for several temperatures, measured for the in-plane diffusivity of Rb in stage-2 RbC_{24} . Solid lines are guides to the eye.

occurs at 1.2 \AA^{-1} . The last fact is demonstrated in Fig. 13, where $S_{\text{coh}}^L(Q)$ and Γ_{coh} are superimposed on the same graph. The structure factor $S_{\text{coh}}^L(Q)$ was again derived from integrating the Lorentzian part of the scattering function over all energies in the limits of $-1.0 \leq E \leq 1.0 \text{ meV}$, and concurs very well with x-ray

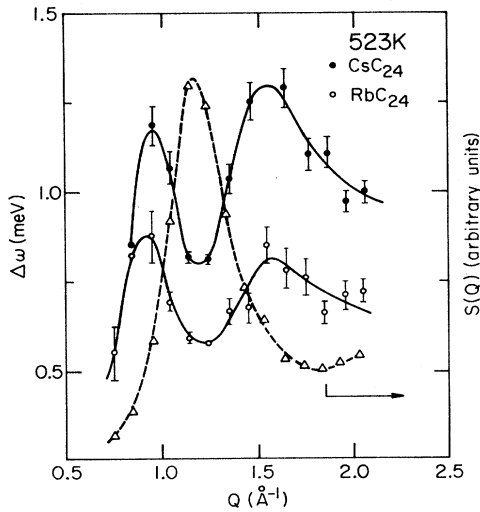


FIG. 13. Lorentzian linewidths for Cs and Rb diffusion in stage-2 graphite intercalation compounds at 523 K. The triangles indicate the structure $S(Q)$ for RbC_{24} at 523 K as obtained by integrating $S(Q, \omega)$ with respect to ω . The solid and dashed lines are guides to the eye.

data of the intercalate liquid structure factor. Figure 13 also shows the Q dependence of the Lorentzian linewidth of CsC_{24} at the same temperature of 523 K. While the Q dependence of the Lorentzian linewidths are similar for both compounds, the Cs values are systematically shifted to higher energies, demonstrating that Cs diffuses faster than Rb at the same temperature.

In the following we compare the Q dependence of Γ_{coh} with simple predictions for continuous and discrete particle motions in order to shed some light on the microscopic diffusion mechanism in the stage-2 compounds. In Fig. 14, experimental points of Γ_{coh} for RbC_{24} (+ symbols) are compared with the quasielastic linewidth that one would expect for a continuously diffusing particle. The initial slopes are matched to yield the same diffusion constant, corresponding to RbC_{24} at a temperature of 523 K. The dashed line represents the calculated incoherent scattering law $\Gamma_{\text{inc}} \propto Q^2$, while the dashed-dotted line reproduces the coherent counterpart Γ_{coh} assuming a liquid structure factor in accord with the alkali-metal intercalate layer. Clearly, the coherent quasielastic linewidth oscillates with decreasing amplitude about the incoherent linewidth, which is expected from the de Gennes effect. While the first minimum at 1.2 \AA^{-1} agrees well with the experimental data points, the

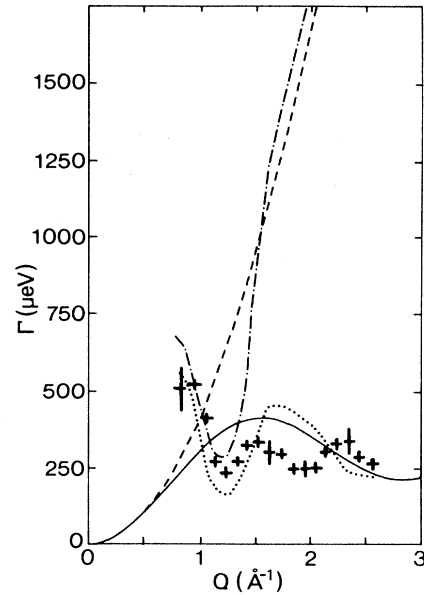


FIG. 14. The measured Lorentzian linewidth as a function of the scattering vector Q for Rb diffusion in RbC_{24} at 523 K (+ symbols) is compared with the linewidth expected for a simple fluid having an incoherent scattering cross section (dashed line) and a coherent scattering cross section (dashed-dotted line). The size of the + symbols corresponds to the experimental error bar. Comparison is also made with a lattice liquid performing jumplike motion to nearest-neighbor sites at a distance of 2.46 \AA , again assuming an incoherent scattering function (solid) and a coherent scattering function (dotted). In all cases the diffusion constant which determines the initial slope at small Q was adjusted to the diffusion constant of Rb in RbC_{24} at 523 K.

mismatch between the predictions for a continuous motion and our actual 2D intercalate liquid becomes intolerable beyond $Q = 1.5 \text{ \AA}^{-1}$.

The other extreme is illustrated by a simple jump-type diffusion process, as is most likely realized in stage-1 compounds. Assuming random jumps between nearest-neighbor hexagon centers at a distance of 2.46 \AA , adjusting the diffusion constant, and taking an appropriate powder average [see Eq. (14)], we obtain an incoherent quasielastic linewidth, which is represented by the solid line in Fig. 14. The coherent linewidth is calculated again by normalizing with the liquid structure factor and is shown as a dotted line in the same figure. We find good agreement between the model calculation and the experimental linewidth in the region from 0.8 to 1.5 \AA^{-1} . However, clear discrepancies occur at 2.0 and 2.4 \AA^{-1} , where the calculated linewidths exhibit a minimum and a maximum, respectively, while the experimental values show just the opposite behavior. The overall discrepancy is however not as large as that for the continuous-diffusion model. A simple adjustment of the jump lengths would not improve the comparison drastically, since the second minimum in the experimental data at 2.0 \AA^{-1} is too narrow to be caused by diffusive jumps. Coherency effects cannot be made responsible for this minimum either, since $S(Q)$ is about 1 at this point. Most likely, there exists a mixture of continuouslike and jumplike diffusive motion within the 2D alkali-metal layer, and the latter may show a distribution of jump lengths, depending on whether the diffusing atoms are closer to the walls or closer to the center of the domains. We also noticed a distinct temperature dependence of the minimum at 2.0 \AA^{-1} , which appears to become more pronounced with increasing temperature, as can be inferred from Fig. 12.

Further detailed studies are required to elucidate the diffusion mechanism in the stage-2 compound and for testing more sophisticated diffusion models. In particular, more data are needed at higher Q values, and also for lower temperatures with increased energy resolution.

4. Pressure dependence

It is well known from the work of Clarke *et al.*⁶³ and Wada⁶⁴ that applying uniaxial pressure along the c axis transforms a stage-2 compound into a stage-3 compound with a $(2 \times 2)R0$ intercalate in-plane structure. The stage transformation starts at about 250 MPa and is completed at about 700 MPa for the $\text{KC}_{24} \rightarrow \text{KC}_{36}$ transformation.

We have studied the quasielastic scattering of RbC_{24} under uniaxial pressure between 0 and 30 MPa, which is far below any pressure-induced staging transformation. The Q dependence of the linewidths at 293 K and for the pressures 0, 3.2, 24, and 30 MPa is shown in Fig. 15. Besides the expected overall decrease of Γ_{coh} with increasing pressure, we also noticed a marked change in the Q dependence of the spectrum. In particular, the maximum at 2.35 \AA^{-1} flattens out at higher pressures, the most dramatic change taking place between ambient pressures and 3 MPa.

The inset of Fig. 15 shows $\Gamma_{\text{coh}}(Q)$ at $Q = 2.35 \text{ \AA}^{-1}$ as

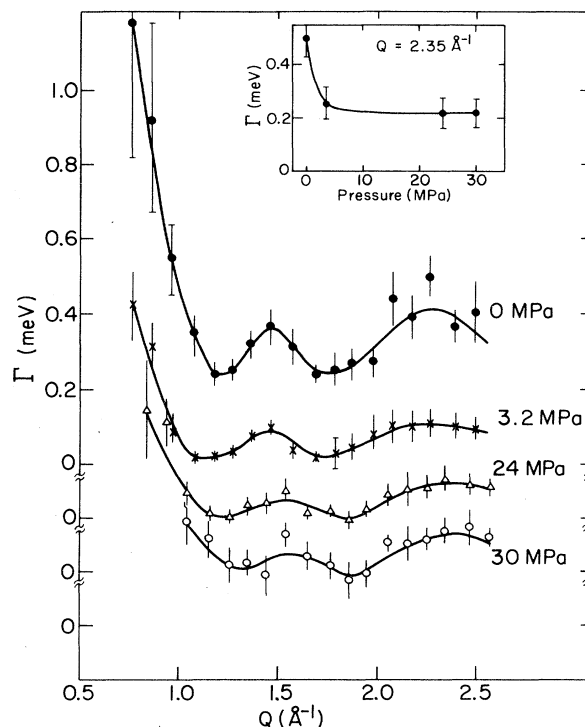


FIG. 15. Lorentzian linewidths for RbC_{24} at 298 K and for several pressures applied uniaxial along the c axis. The inset shows the pressure dependence of Lorentzian spectra at $Q = 2.35 \text{ \AA}^{-1}$ and at 298 K. All lines are guides to the eye.

a function of pressure. As mentioned before, the most drastic change occurs at small pressures, while the width remains constant from 3 to 30 MPa. From this we can conclude that at low pressures an important contribution to the diffusivity becomes blocked almost immediately. Naively one would expect that any continuouslike diffusivity is affected most strongly by the application of pressure, and that the jumplike motion survives until much higher pressures are applied. However, neither the oscillation of the quasielastic linewidth nor the structure factor $S(Q)$ conform to such a simple notion. It appears that the diffusive paths of the alkali-metal atoms on the hexagonal graphite substrate are much more complex and far from being solved.

5. Diffusion constants

In spite of coherency effects, the diffusion constant for the intercalate layers can be determined via procedures discussed previously. In the case of stage-2 compounds, we estimate that $S(Q) \cong 1.0$ at about 1.1 \AA^{-1} for all three stage-1 compounds. Using the intrinsic width Γ at this point, we can calculate the diffusion constant using Eq. (6). Figure 16 shows Arrhenius plots of the diffusion constants for K, Rb, and Cs. It should be noted that in all three cases the diffusion can be well described by a single activation energies, listed in Table III together with their prefactors D_0 . The description of the diffusion process

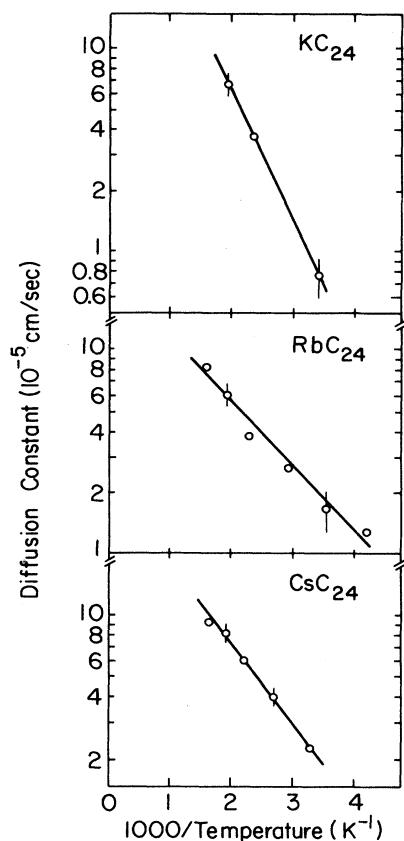


FIG. 16. Arrhenius plots of the diffusion constants for the three stage-2 compounds KC_{24} , RbC_{24} , and CsC_{24} . The linear slopes are least-squares fits to the data points yielding activation energies for the alkali-metal in-plane diffusivity listed in Table III.

by a single-valued activation energy is a bit surprising in view of the complexity of the intercalate motion.

DiVincenzo and Mele³¹ argue that the potential barrier to the diffusion should be about the same in stage-1 and -2 compounds, whereas we observe a rather drastic reduction. For instance, the activation energy for KC_8 is 0.18 eV and drops to 0.126 eV in KC_{24} . Because of missing data, similar comparisons cannot be made for the Rb and Cs intercalation compounds. We believe, however, that the structural differences between stage-1 and -2 compounds hints at a reduced alkali-metal-graphite interaction in the stage-2 compounds, and that the activation energies listed in Table III reflect this trend. Moss *et al.*³³ find from an x-ray analysis of the graphite substrate potential in RbC_{24} an energy difference of 0.092 eV between the potential minimum in the center of the graphite hexagon and the saddle point between two carbon atoms along their bond. This value has to be compared with the activation energy of 0.063 eV, which we have obtained from the present quasielastic data. If the Rb atoms in the stage-2 compounds were performing jumps from hexagon to hexagon site, the barrier energy

of 0.092 eV would apply. However, because of the inequivalency of the lattice sites and the smearing out of the positions, some atoms experience much smaller potential barriers. The trend to a lower averaged barrier height seems to be reflected by the activation energy obtained from the diffusion data.

It is also interesting to note that the prefactor D_0 increases systematically with increasing alkali-metal mass. While the activation energy is slightly higher for Cs than for Rb, it is the prefactor which causes Cs to diffuse faster than Rb in the stage-2 compounds and in the temperature range considered here. For a lattice-liquid-type diffusion the prefactor can be written in simplified notation:⁶⁵ $D_0 = \omega l^2 \exp(-\Delta S/k_B)$, where ω is the particle frequency or attempt frequency, l is the jump distance, and ΔS is the change of the entropy between the saddle point and the potential minimum. Assuming that l is the same for all three stage-2 compounds, the changes of D_0 must either be caused by ω or by ΔS . Since the frequencies of the intercalate in-plane modes decrease with increasing alkali-metal mass,²⁶ the present behavior can only be explained by a decreasing entropy change in the sequence from K to Cs. This could be seen as an indication for Cs having a smaller available number of diffusion paths starting from the saddle point than the light alkali-metal atoms, possibly due to size effects.

On an absolute scale the diffusion constants which we find for the alkali-metal atoms in graphite are much smaller than those of the free 3D liquids,²⁸ but they are of the same order of magnitude as those measured for hydrogen in metals⁶⁶ and for superionic conductors.⁶⁷

V. DISCUSSION AND SUMMARY

The present QENS studies indicate that in stage-1 alkali-metal graphite intercalation compounds the diffusive motion of the intercalate atoms proceeds via jumps on lattice sites provided by the graphite substrate. This has been clearly demonstrated for LiC_6 , but is also expected for the other heavy alkali-metal stage-1 compounds. Here, coherency effects have prevented us from extracting jump vectors. The self-diffusion constants and activation energies for the stage-1 compounds are in line with the general notion that the intercalate-graphite interaction is rather strong in these systems. This is particularly true for LiC_6 , which exhibits the highest activation energy of about 1 eV. Phonon dispersion measurements have also demonstrated that LiC_6 is the least anisotropic compound among the alkali-metal GIC's.⁴²

The stage-2 alkali-metal GIC's represent systems of far greater complexity. At the same time they offer a perfect laboratory for investigating the intriguing problem of the dynamics of a 2D melting process on a corrugated substrate. One of the most important results of our QENS experiments is the observation that the 2D melting process on periodic substrates is very smooth, stretching over a wide temperature range. During this transformation, a solidlike δ component and a liquidlike Lorentzian

component in the dynamical structure factor coexist and exchange intensity with increasing temperature. This behavior could not have been conjectured by merely measuring the structure factor, which shows a normal, second-order-type phase transition and a liquidlike state above the structural transition temperatures. Only a full Q and ω analysis of the structure factor reveals the rich facets of this melting transition.

We believe that the L component originates from diffusing particles within disordered regions, whereas the δ component is due to atoms residing more rigidly within the substrate potential wells. The coexistence of these two parts in thermal equilibrium above the structural melting transition is an entirely new phenomenon not known for simple 3D systems. In 3D monatomic liquids such as the free alkali metals, a δ component does not exist for any temperature in the liquid phase.^{28,29} The present results on the 2D melting process must also be distinguished from a heterogeneous liquid-solid phase coexistence along a liquidus-solidus line, in which case one would expect the coexistence of a solidlike and liquidlike structure factor. The new phenomenon discussed here is the coexistence of two different dynamic structure factors for one and the same static structure factor. We argue that this dynamical behavior is unique to the melting process of a 2D incommensurate domain lattice on a periodic substrate. Because of the inequivalency of the lattice sites, the melting transition is characteristically slow, starting first at the domain walls and then proceeding further into the centers of the more ordered domains. The continuous nature of the melting process is also expressed by the small specific-heat anomaly at T_c .⁶⁸ With increasing temperature the diffusive motion of the alkali-metal atoms becomes more dominant and the alkali-metal layers transform into rotationally isotropic 2D liquids. This process is profoundly different from the melting in three dimensions. A similar behavior has recently also been observed for the melting of a two-dimensional molecular layer in graphite.¹⁰

In an independent inelastic-neutron-scattering work, Kamitakahara and Zabel²⁶ have shown that, above the disordering temperature, transverse and longitudinal phononlike in-plane modes from the intercalate layers exist, and that those modes persist to high temperatures above the melting temperatures. The phononlike modes are intimately related to the presence of δ -like component in the dynamical structure factor, because only atoms which reside for a certain amount of time in a potential well are able to perform harmonic oscillations. The phononlike character of these modes requires that the "rigid" atoms cluster together in patches in order to support transverse as well as longitudinal excitations.

Melting in 2D incommensurate solids by domain-wall oscillations and formation of free dislocations has been predicted by Coppersmith *et al.*⁶⁹ and has also been seen in molecular-dynamics simulations by Abraham *et al.*⁷⁰ A molecular-dynamics simulation with the proper pair potentials and intercalate densities for Rb in stage-2 graphite has recently been provided by Fan, Reiter, and Moss.³⁰ Their simulation not only reproduces the static structure factor $S(Q)$ in very good agreement with exper-

iments, but also a dynamical structure factor composed of a δ -function part and a Lorentzian part. They could show that in the presence of the substrate potential indeed a δ and a Lorentzian part coexist in the disordered phase and the solidlike part is long-lived enough to give rise to transverse and longitudinal phononlike excitations.

The most important effect of the incommensurate substrate potential is the tendency to cluster atoms into domains of approximate registry with the underlying periodicity. These patches of atoms are separated by domain walls in which structural phase slips occur. In the ordered state those domains arrange in a periodic fashion and the resulting structure is referred to as a discommensuration structure (see Fig. 8). In the liquid state these domains continue to exist, but now with a much reduced coherence length and in a more dynamical sense. That is, atoms which are at one time within one domain taking part in the lattice vibration may at another time be outside and performing diffusive motion. The existence of domains induced by the substrate potential provides the most important distinction between a simple liquid and a modulated liquid. In a modulated liquid, as long as the temperature is not too high to destroy the domains, solidlike phonon excitations exist for all Q values and have longitudinal as well as transverse components, while in simple liquids only longitudinal density fluctuations exist and their wave vectors are limited to a small region up to the maximum of the LSF, at which point a distinction between vibrational and diffusive excitation starts to fail.

Phase coexistence of solidlike and liquidlike patches has also been observed in constant-density Lennard-Jones MC simulations of the 2D melting transition without a substrate potential. The interpretation of these patches, however, remains controversial and could either be taken as artifacts of the computer simulation or as signatures of critical fluctuations expected in hexatic phases. In an excellent review paper on this subject, Strandburg⁷¹ suggests that one should apply in the simulation a sixfold potential, which is then removed to test the stability of the coexisting phases. In the present case of intercalates in graphite this potential is provided by the host substrate, and the coexistence of liquidlike and solidlike domains is clearly induced by the corrugated substrate. The MD simulation of Fan *et al.*³⁰ indicates that the δ or solidlike part disappears together with the phononlike excitations when the graphite host corrugation potential is decreased.

In summary, through quasielastic-neutron-scattering experiments we have observed that alkali-metal atoms perform lattice liquidlike hopping motions in stage-1 intercalation compounds, where the alkali-metal-layer structure is commensurate with the substrate and the graphite-alkali-metal interaction relatively strong. For stage-2 compounds, which display discommensuration domain lattices, we have analyzed for the first time the dynamics of the melting of two-dimensional layers on a periodic substrate. We have noticed that the melting transition in the presence of a corrugated host potential is characteristically slow, extending over several hundreds

of degrees centigrade with solidlike and liquidlike excitations coexisting. With increasing temperature, the liquidlike diffusional mobility gains over phononlike excitations, and the two-dimensional static liquid structure factor gradually becomes in-plane isotropic. This melting process is distinctively different from the melting in three dimensions. We have also obtained diffusion constants and activation energies for most of the stage-1 and -2 compounds.

ACKNOWLEDGMENTS

Stimulating discussions with A. Dianoux, M. Suzuki, S. C. Moss, G. Reiter, and J. M. Rowe are gratefully acknowledged. The work at The University of Illinois at Urbana-Champaign was supported by the U.S. National Science Foundation under Grant No. DMR-86-05565, which is gratefully acknowledged.

*Present address: Experimentalphysik IV, Ruhr Universität Bochum, D-4630 Bochum 1, West Germany.

†Present address: Materials Science Program, University of Wisconsin, Madison, WI 53706.

¹For recent short reviews of some of the aspects of graphite intercalation compounds, see H. Zabel and P. C. Chow, *Comments Condensed Matter Phys.* **12**, 225 (1986); H. Kamimura, *Physics Today* **40**(12), 64 (1987).

²T. Springer, in *Quasielastic Neutron Scattering for the Investigation of Diffusive Motion in Solids and Liquids*, Vol. 64 of *Springer Tracts in Modern Physics*, edited by G. Höhler (Springer, Berlin, 1972).

³T. Springer and D. Richter, in *Neutron Scattering*, edited by D. L. Price and K. Sköld (Academic, San Diego, 1987), Pt. B, Vol. 23.

⁴H. Zabel, in *Nontraditional Methods in Diffusion*, edited by G. E. Murch, H. K. Birnbaum, and J. R. Cost (The Metallurgical Society of AIME, Warrendale, PA, 1983), p.1

⁵S. A. Solin, *Adv. Chem. Phys.* **49**, 455 (1982).

⁶R. Moret, in *Intercalation in Layered Materials*, edited by M. S. Dresselhaus, NATO Advanced Study Institute Series B: *Physics* (Plenum, New York, 1986), Vol. 148, p. 185.

⁷S. C. Moss and R. Moret, in *Graphite Intercalation Compounds, Vol. 1: Structure and Dynamics*, Topics in Current Physics, edited by H. Zabel and S. A. Solin, (Springer-Verlag, Berlin, in press).

⁸D. A. Neumann, H. Zabel, Y. B. Fan, S. A. Solin, and J. J. Rush, *Phys. Rev. B* **37**, 8424 (1988).

⁹D. A. Neumann and H. Zabel, *Can. J. Chem.* **66**, 666 (1988).

¹⁰I. Rosenman, Ch. Simon, F. Batallan, and A. Magerl, *Europhys. Lett.* **3**, 1013 (1987).

¹¹A. Magerl, in *Graphite Intercalation Compounds, Vol. 1: Structure and Dynamics*, Ref. 7.

¹²G. Kirzenow, *Synth. Met.* **23**, 1 (1988).

¹³M. E. Misenheimer and H. Zabel, *Phys. Rev. B* **27**, 1443 (1983).

¹⁴R. Nishitani, Y. Uno, and H. Suematsu, *Phys. Rev. B* **27**, 6572 (1983).

¹⁵R. Nishitani, Y. Sasaki, and Y. Nishina, *Phys. Rev. B* **37**, 3141 (1988).

¹⁶P. Hernandez, F. Lamelas, R. Clarke, P. Dimon, E. B. Sirota, and S. K. Sinha, *Phys. Rev. Lett.* **59**, 1220 (1987).

¹⁷F. C. Frank and J. H. van der Merwe, *Proc. R. Soc. London, Ser. A* **198**, 205 (1949).

¹⁸A. Bunde and W. Dietrich, *Solid State Commun.* **37**, 229 (1981).

¹⁹M. Plischke, *Can. J. Phys.* **59**, 802 (1981).

²⁰G. S. Parry, *Mater. Sci. Eng.* **31**, 99 (1977).

²¹F. Rousseaux, R. Moret, D. Guerard, P. Lagrange, and M. Lelaurain, *Synth. Met.* **12**, 45 (1985).

²²G. Reiter and S. C. Moss, *Phys. Rev. B* **33**, 7209 (1986).

²³M. Plischke and W. D. Leckie, *Can. J. Phys.* **60**, 1139 (1982).

²⁴D. P. DiVincenzo, *Synth. Met.* **12**, 111 (1985).

²⁵Z.-M. Chen, O. A. Karim, and B. M. Pettitt, *J. Chem. Phys.* **89**, 1042 (1988).

²⁶W. A. Kamitakahara and H. Zabel, *Phys. Rev. B* **32**, 7817 (1985).

²⁷J. W. White and P. A. Wielopolski, *Phys. Rev. B* **36**, 6069 (1987).

²⁸R. D. Copley and J. M. Rowe, *Phys. Rev. A* **9**, 1656 (1974).

²⁹R. D. Copley and S. W. Lovesey, *Rep. Prog. Phys.* **38**, 461 (1975).

³⁰J. D. Fan, G. Reiter, and S. C. Moss, in *Graphite Intercalation Compounds: Science and Applications*, Materials Research Society Extended Abstracts, edited by M. Endo, M. S. Dresselhaus, and G. Dresselhaus (MRS, Pittsburgh, 1988), p. 13.

³¹D. P. DiVincenzo and E. J. Mele, *Phys. Rev. B* **32**, 2538 (1985).

³²C. Thompson, S. C. Moss, G. Reiter, and M. E. Misenheimer, *Synth. Met.* **12**, 57 (1985).

³³S. C. Moss, G. Reiter, J. L. Robertson, C. Thompson, J. D. Fan, and K. Ohshima, *Phys. Rev. Lett.* **57**, 3191 (1986).

³⁴H. Zabel, A. Magerl, J. J. Rush, and A. J. Dianoux, in *Intercalated Graphite*, Mater. Res. Soc. Symp. Proc. No. 20, edited by M. S. Dresselhaus, G. Dresselhaus, J. E. Fischer, and M. J. Moran (North-Holland, New York, 1983), p. 289.

³⁵H. Zabel, A. Magerl, A. J. Dianoux, and J. J. Rush, *Phys. Rev. Lett.* **50**, 2094 (1983).

³⁶A. Magerl, H. Zabel, and I. S. Anderson, *Phys. Rev. Lett.* **55**, 222 (1985).

³⁷H. Zabel, S. E. Hardcastle, D. A. Neumann, M. Suzuki, and A. Magerl, *Phys. Rev. Lett.* **57**, 2041 (1986).

³⁸H. Zabel, M. Suzuki, D. A. Neumann, S. E. Hardcastle, A. Magerl and W. A. Kamitakahara, *Synth. Met.* **12**, 105 (1985).

³⁹S. W. Lovesey, *Theory of Neutron Scattering from Condensed Matter* (Clarendon, Oxford, 1984), Vol. I.

⁴⁰V. F. Sears, in *Neutron Scattering*, edited by K. Sköld and D. L. Price (Academic, San Diego, 1986), Pt. A, Vol. 23.

⁴¹K. Sköld, *Phys. Rev. Lett.* **19**, 1023 (1967).

⁴²H. Zabel, A. Magerl, and J. J. Rush, *Phys. Rev. B* **27**, 3930 (1983).

⁴³User Manual, Neutron Beam Facilities, Institut-Laue-Langevin, Grenoble, France, 1988 (unpublished).

⁴⁴J. Rossat-Mignod, A. Wiedemann, K. C. Woo, J. W. Milliken, and J. E. Fischer, *Solid State Commun.* **44**, 1339 (1982).

⁴⁵D. S. Robinson and M. B. Salamon, *Phys. Rev. Lett.* **48**, 156 (1982).

⁴⁶J. E. Fischer and H. J. Kim, *Phys. Rev. B* **35**, 3295 (1987).

⁴⁷H. J. Kim, A. Magerl, J. L. Soubeyroux, J. E. Fischer, and D.

- Vaknin, in *Graphite Intercalation Compounds: Science and Applications*, Ref. 30, p. 5.
- ⁴⁸P. Freilander, P. Heitjans, H. Ackermann, B. Bader, G. Kiese, A. Schirmer, H. J. Stöckmann, C. van der Marel, A. Magerl, and H. Zabel, *Z. Phys. Chem., Neue Folge* **151**, 93 (1987).
- ⁴⁹H. Estrade, J. Conard, P. Lauginie, P. Heitjans, F. Fujara, W. Buttler, G. Kiese, A. Ackermann, and D. Guérard, *Physica (Amsterdam)* **99B**, 531 (1980).
- ⁵⁰H. Minemoto and H. Suematsu, *Synth. Met.* **12**, 33 (1985).
- ⁵¹N. Metoki and H. Suematsu, *Phys. Rev. B* **38**, 5310 (1988).
- ⁵²W. D. Ellenson, D. Semmingsen, D. Guerard, D. G. Onn, and J. E. Fischer, *Mater. Sci. Eng.* **31**, 137 (1977).
- ⁵³D. S. Robinson, T. C. McGlenn, J. L. Zarestky, and M. B. Salamon, in *Graphite Intercalation Compounds*, Extended Abstracts of the Materials Research Society Symposium Proceedings, edited by M. S. Dresselhaus, G. Dresselhaus, and S. A. Solin (MRS, Pittsburgh, 1986), p. 16.
- ⁵⁴R. Clarke, N. Caswell, and S. A. Solin, *Phys. Rev. Lett.* **42**, 61 (1979).
- ⁵⁵J. B. Hastings, W. D. Ellenson, and J. E. Fischer, *Phys. Rev. Lett.* **42**, 1552 (1979).
- ⁵⁶R. Clarke, N. Caswell, S. A. Solin, and P. M. Horn, *Phys. Rev. Lett.* **43**, 2018 (1979).
- ⁵⁷H. Zabel, S. C. Moss, N. Caswell, and S. A. Solin, *Phys. Rev. Lett.* **43**, 2022 (1979).
- ⁵⁸M. Suzuki, H. Ikeda, H. Suematsu, Y. Endoh, H. Shiba, and M. T. Hutchings, *J. Phys. Soc. Jpn.* **49**, 671 (1980).
- ⁵⁹M. J. Winokur and R. Clarke, *Phys. Rev. Lett.* **54**, 811 (1985).
- ⁶⁰M. Suzuki and H. Suematsu, *J. Phys. Soc. Jpn.* **52**, 2761 (1983).
- ⁶¹M. Suzuki, *Phys. Rev. B* **33**, 1386 (1986).
- ⁶²C. Thompson, Ph.D. thesis, University of Houston, 1987.
- ⁶³R. Clarke, N. Wada, and S. A. Solin, *Phys. Rev. Lett.* **44**, 1616 (1980).
- ⁶⁴N. Wada, *Phys. Rev. B* **24**, 1065 (1981).
- ⁶⁵C. P. Flynn, *Point Defects and Diffusion* (Clarendon, Oxford, 1972).
- ⁶⁶J. Völkl and G. Alefeld, in *Hydrogen in Metals*, Vol. 1 of *Topics in Applied Physics*, edited by G. Alefeld and J. Völkl (Springer-Verlag, Berlin, 1978), p. 321.
- ⁶⁷S. M. Shapiro and F. Reidinger, in *Superionic Conductors*, Vol. 15 of *Topics in Current Physics*, edited by M. B. Salamon (Springer-Verlag, Berlin, 1979), p. 45.
- ⁶⁸H. Suematsu, M. Suzuki, and H. Ikeda, *J. Phys. Soc. Jpn.* **49**, 835 (1980).
- ⁶⁹S. N. Coppersmith, D. S. Fisher, B. I. Halperin, P. A. Lee, and W. F. Brinkman, *Phys. Rev. B* **25**, 349 (1982).
- ⁷⁰F. F. Abraham, S. W. Koch, and W. E. Rudge, *Phys. Rev. Lett.* **49**, 1830 (1982).
- ⁷¹K. J. Strandburg, *Rev. Mod. Phys.* **60**, 161 (1988).